CHEMISTRY
A EUROPEAN JOURNAL

DOI: 10.1002/chem.200501490

Solid-State NMR and EXAFS Spectroscopic Characterization of Polycrystalline Copper(I) *O,O′*-Dialkyldithiophosphate Cluster Compounds: Formation of Copper(I) *O,O′*-Diisobutyldithiophosphate Compounds on the Surface of Synthetic Chalcocite

Daniela Rusanova,[a] Kevin J. Pike,[b] Ingmar Persson,*[c] John V. Hanna,[b] Ray Dupree,[d] Willis Forsling,[a] and Oleg N. Antzutkin*[a]

Abstract: A number of polycrystalline copper(I) *O,O′*-dialkyldithiophosphate cluster compounds with Cu_4, Cu_6, and Cu_8 cores were synthesized and characterized by using extended X-ray absorption fine-structure (EXAFS) spectroscopy. The structural relationship of these compounds is discussed. The polycrystalline copper(I) *O,O′*-diisobutyldithiophosphate cluster compounds, $[Cu_8\{S_2P(OiBu)_2\}_6(S)]$ and $[Cu_6\{S_2P(OiBu)_2\}_6]$, were also characterized by using ^{31}P CP/MAS NMR (CP = cross polarization, MAS = magic-angle spinning) and static ^{65}Cu NMR spectroscopies (at different magnetic fields) and powder X-ray diffraction (XRD) analysis. Comparative analyses of the ^{31}P chemical-shift tensor, and the ^{65}Cu chemical shift and quadrupolar-splitting parameters, estimated from the experimental NMR spectra of the polycrystalline copper(I) cluster compounds, are presented. The adsorption mechanism of the potassium *O,O′*-diisobutyldithiophosphate collector, $K[S_2P(OiBu)_2]$, at the surface of synthetic chalcocite (Cu_2S) was studied by means of solid-state ^{31}P CP/MAS NMR spectroscopy and scanning electron microscopy (SEM). ^{31}P NMR resonance lines from collector-treated chalcocite surfaces were assigned to a mixture of $[Cu_8\{S_2P(OiBu)_2\}_6(S)]$ and $[Cu_6\{S_2P(OiBu)_2\}_6]$ compounds.

Keywords: adsorption · chalcocite · cluster compounds · copper · EXAFS spectroscopy · NMR spectroscopy

Introduction

Copper(I) and copper(II) complexes with 1,1-dialkyldithio ligands have been extensively studied because of their use in a wide range of applications in industry (e.g., selective flotation agents,[1] antioxidants for motor oils[2]), agriculture (e.g., insecticides and pesticides[3]), and science (e.g., analytical reagents for extraction and spectrophotometric determination of metal ions[4]). Copper(I) *O,O′*-dialkyldithiophosphate compounds are polynuclear and contain only chelating-type ligands, which bridge two or more metal ions. The internal oxidation of the ligand to bis(thiophosphoryl) disulfide with a concomitant reduction of copper(II) to copper(I)[5] leads to the formation of copper(I) cluster compounds, or cage molecules, containing Cu_4 (tetrahedral), Cu_6 (trigonal antiprismatic), or Cu_8 (cubic) cores in which the copper(I) ions reside in a trigonal plane formed by sulfur atoms. Due to difficulties in producing single crystals amenable to X-ray diffraction, or the inability to distinguish between similar clusters by conventional spectroscopic methods, a limited number of the copper(I) *O,O′*-dialkyldithiophosphate clus-

[a] D. Rusanova, Prof. W. Forsling, Assoc. Prof. O. N. Antzutkin
Division of Chemistry
Luleå University of Technology
971 87 Luleå (Sweden)
Fax: (+46) 920-491-199
E-mail: Oleg.Antzutkin@ltu.se

[b] Dr. K. J. Pike, Dr. J. V. Hanna
ANSTO NMR Facility
c/o Institute of Materials & Engineering Science
Lucas Heights Research Laboratories
Private Mail Bag 1, Menai NSW 2234 (Australia)

[c] Prof. I. Persson
Department of Chemistry
Swedish University of Agricultural Sciences
P.O. Box 7015, 750 07 Uppsala (Sweden)
Fax: (+46) 186-73-476
E-mail: Ingmar.Persson@kemi.slu.se

[d] Prof. R. Dupree
Department of Physics
University of Warwick
Coventry CV4 7AL (UK)

Supporting information for this article is available on the WWW under http://www.chemeurj.org/ or from the author.

ters have been characterized crystallographically.[6–12] Only one structure for each of the first two classes of clusters has been crystallographically characterized, $[Cu_4\{S_2P(OiPr)_2\}_4]$[7] and $[Cu_6\{S_2P(OEt)_2\}_6]$,[8] whereas seven structures with the octameric architecture, $[Cu_8\{S_2P(OR)_2\}_6(X)]$ (R = Et, *n*Pr, *i*Pr; X = S^{2-}, Cl^-, Br^-), have been reported.[6,8–12] The octanuclear clusters require a central anion X (S^{2-}, Br^-, Cl^-) to reduce the charge and in the case of the centered halides, a positively charged $[Cu_8L_6(X)]^+$ cluster ion is formed. The sulfide-containing cluster $Cu_8L_6(S)$, and the Cu_4L_4 and Cu_6L_6 (L = $S_2P(OR)_2$, R = alkyl) cluster compounds are neutral.

To the best of our knowledge, the flotation recovery, contact angle measurements, and electrochemical and wetting behavior of chalcocite (Cu_2S) in aqueous solution have been studied only with reference to potassium *O*,*O*′-diethyldithiophosphate, used as the collector in the differential flotation of mixed sulfide ores: Cu–Zn, Co–Ni and Cu–Co.[13,14] The same collector was used when the surface was examined by using DRIFT spectroscopic analysis.[15] However, data for other collectors such as potassium *O*,*O*′-diisobutyl-, -isoamyl-, and -*o*-cresyldithiophosphates, widely used in mono-flotation of sulfide copper and silver ores and native gold, have not been reported and the mechanisms of the surface complexation or precipitation of polycrystalline phases have not yet been described and are not known.

In our previous work we have reported the solid-state ^{31}P CP/MAS NMR (CP = cross polarization, MAS = magic-angle spinning) and ^{65}Cu NMR spectroscopic data for the tetranuclear $[Cu_4\{S_2P(OiPr)_2\}_4]$, hexanuclear $[Cu_6\{S_2P(OEt)_2\}_6]$, and a few octanuclear copper(I) *O*,*O*′-dialkyldithiophosphate cluster compounds.[10,16,17] We have recorded copper K-edge extended X-ray absorption fine structure analysis (EXAFS) data for a series of octanuclear *O*,*O*′-dialkyldithiophosphate cluster compounds and discussed the stability of the $Cu_8S_{12}(S)$ core.[10]

This paper presents EXAFS analyses on polynuclear copper(I) *O*,*O*′-dialkyldithiophosphate clusters with different core compositions (Cu_4, Cu_6, and Cu_8 cores) and their structural relationships. The clusters with known structures, tetranuclear $[Cu_4\{S_2P(OiPr)_2\}_4]$, hexanuclear $[Cu_6\{S_2P(OEt)_2\}_6]$, octanuclear $[Cu_8\{S_2P(OR)_2\}_6(S)]$ (R = Et, *n*Pr, *i*Pr), and two polycrystalline cluster compounds with still unknown structures, $[Cu_8\{S_2P(OiBu)_2\}_6(S)]$ (**1**) and $[Cu_6\{S_2P(OiBu)_2\}_6]$ (**2**), are examined. The last two were also characterized using ^{31}P CP/MAS (at 8.46 T) and static ^{65}Cu NMR (at 14.1 T) spectroscopies, and powder X-ray diffraction (XRD) analysis. Comparative analyses of the ^{31}P chemical-shift tensors, and the ^{65}Cu chemical shift and quadrupolar-splitting parameters that were estimated from the NMR spectra are given. The solid-state ^{65}Cu NMR spectra of **1** at 7.05 and 9.4 T are also provided and were used to increase the accuracy of the ^{65}Cu spectral parameters obtained from simulations of these spectra.

As previously reported, ^{31}P chemical shifts can be successfully used for the assignment of the coordination mode (bridging or terminal) of *O*,*O*′-dialkyldithiophosphate ligands adsorbed on the surface of synthetic sphalerite and galena.[18] The same approach was applied in our studies of the adsorption of potassium *O*,*O*′-diethyldithiophosphate on the surface of synthetic chalcocite.[17] In this paper, we extend this approach for the synthetic chalcocite by applying another potassium *O*,*O*′-dialkyldithiophosphate collector, $K[S_2P(OiBu)_2]$. The morphological changes observed on the chalcocite surfaces treated with different concentrations of this collector and the assignment of the species formed at the mineral surface were monitored using scanning electron microscopy (SEM) and ^{31}P CP/MAS NMR spectroscopy.

Results and Discussion

Structures of copper(I) *O*,*O*′-dialkyldithiophosphate cluster compounds: In the crystal structure of the tetranuclear cluster compound $[Cu_4\{S_2P(OiPr)_2\}_4]$,[7] each copper(I) ion is bound to three sulfur atoms, forming a triangle, with the copper ion in the center, and a mean Cu–S bond length of 2.267 Å. Each of the four *O*,*O*′-diisopropyldithiophosphate ligands bridges three copper(I) ions and displays a trimetallic triconnective pattern: one of the sulfur atoms binds to one copper ion while the second is bound to two.[19] The copper(I) ions themselves form a somewhat distorted tetrahedron with a mean Cu···Cu distance of 2.81 Å. $[Cu_4\{S_2P(OiPr)_2\}_4]$ crystallizes in an orthorhombic space group, $P2_12_12_1$.

In the only crystallographically characterized hexanuclear cluster, $[Cu_6\{S_2P(OEt)_2\}_6]$, the ligands also display a trimetallic triconnective coordination mode with sulfur atoms bound to either one or two copper ions, with somewhat shorter Cu–S bond lengths (2.250 Å).[8] The six copper(I) ions form a trigonal antiprismatic configuration with a mean Cu···Cu distance of 3.129 Å. $[Cu_6\{S_2P(OEt)_2\}_6]$ crystallizes in a space group with a high symmetry, $R\bar{3}$ (trigonal).

The architectures of the octameric clusters, $[Cu_8\{S_2P(OR)_2\}_6(X)]$ (R = alkyl; X = S^{2-}, Cl^-, or Br^-), are different: the ligand displays the rare tetrametallic tetraconnective coordination pattern: each *O*,*O*′-dialkyldithiophosphate ligand bridges four copper(I) ions and every sulfur atom is bound to two copper(I) ions.[19] Each of the copper(I) ions is bound to three sulfur atoms and is positioned slightly above the S_3 plane. The average S-Cu-S angle is about 119° and the mean Cu–S bond length is 2.29 Å. In addition, all copper centers are also attached to the central sulfide, chloride, or bromide ion, perpendicular to the CuS_3 planes, thus completing a triangular pyramidal configuration around the copper(I) ions. The eight copper(I) ions form a cubic configuration with a mean Cu···Cu distance that increases with increasing size of the central ions: 3.01 (3.11 for $[Cu_8\{S_2P(OiPr)_2\}_6(S)]$[8]), 3.11, and 3.17 Å for the sulfide, chloride, and bromide analogues, respectively.[8–11] $[Cu_8\{S_2P(OEt)_2\}_6(S)]$ and $[Cu_8\{S_2P(OnPr)_2\}_6(S)]$ crystallize in a space group with a high symmetry, $R\bar{3}$ (trigonal), while the $[Cu_8\{S_2P(OiPr)_2\}_6(S)]$, $[Cu_8\{S_2P(OiPr)_2\}_6(Cl)]PF_6$, and $[Cu_8\{S_2P$-

$(OiPr)_2\}_6(Br)]PF_6$ cluster compounds have lower symmetries, *C*2/*c* (monoclinic).

In the structural configuration of $[Cu_6\{S_2P(OEt)_2\}_6]$ it can be seen that two copper atoms across a cubic diagonal and the central counter ion in the $Cu_8S_{12}(S)$ core are omitted and it is somewhat surprising that the average Cu···Cu distance in the former is longer than that in the $Cu_8S_{12}(S)$ core in $[Cu_8\{S_2P(OR)_2\}_6S]$. Measurements on the icosahedron ligand shell show that it undergoes a slight shrinkage of 0.156 Å when these copper atoms are removed. For the $[Cu_8\{S_2P(OR)_2\}_6S]$ cluster compound, with R = Et, *n*Pr, and *i*Pr,[8–10] it was found that the ligand shell remains fairly constant and the changes are within 0.02 Å.

The average Cu···Cu distances and Cu–S and Cu–S_{center} bond lengths calculated from the aforementioned crystallographic structures, together with the EXAFS data (see below), are shown in Table 1.

EXAFS studies of copper(I) *O*,*O*′-dialkyldithiophosphate cluster compounds—the structural relationship between the polynuclear clusters with different copper cores (Cu_4, Cu_6, Cu_8): EXAFS is a lattice-independent structure method, which provides information about the structure around the absorbing atom in the sample (in this case, copper). The copper K-edge EXAFS data for the polycrystalline samples of the $[Cu_4\{S_2P(OiPr)_2\}_4]$, $[Cu_6\{S_2P(OEt)_2\}_6]$, $[Cu_8\{S_2P(OEt)_2\}_6(S)]$, $[Cu_8\{S_2P(OnPr)_2\}_6(S)]$, and $[Cu_8\{S_2P(OiPr)_2\}_6(S)]$ cluster compounds with known structures, and $[Cu_8\{S_2P(OiBu)_2\}_6(S)]$ (**1**) and $[Cu_6\{S_2P(OiBu)_2\}_6]$ (**2**) with still unknown structures are shown in Figure 1. The fits of the EXAFS data are also shown in Figure 1, and the individual scattering path contributions can be also found in the Supporting Information.

The cluster compounds display similar EXAFS functions with only very small differences between the different types of structures.

The structure parameters for the tetranuclear cluster compound, $[Cu_4\{S_2P(OiPr)_2\}_4]$, from X-ray crystallography and EXAFS data are the same within the error limits: the mean Cu–S bond length is 2.265 Å and the mean Cu···Cu distance is 2.81 Å (see Table 1).

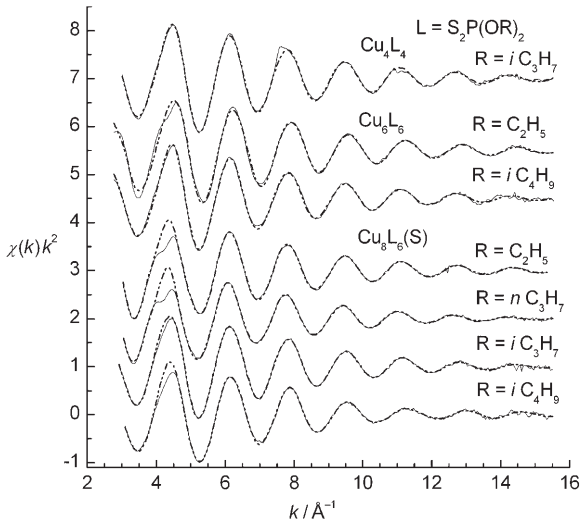

Figure 1. The fit of the EXAFS data for cluster compounds **1** (no offset), $[Cu_8\{S_2P(OiPr)_2\}_6(S)]$ (offset 1.0), $[Cu_8\{S_2P(OnPr)_2\}_6(S)]$ (offset 1.5), $[Cu_8\{S_2P(OEt)_2\}_6(S)]$ (offset 2.7), **2** (offset 5.0), $[Cu_6\{S_2P(OEt)_2\}_6]$ (offset 6.0), and $[Cu_4\{S_2P(OiPr)_2\}_4]$ (offset 7.0). Solid lines = experimental data; dashed lines = model.

The pairs of values obtained by means of X-ray crystallography and EXAFS for the hexanuclear cluster compound $[Cu_6\{S_2P(OEt)_2\}_6]$, however, are significantly different and not within the error limits. The EXAFS data show a mean Cu–S bond length of 2.266(3) Å and a mean Cu···Cu distance of 2.85(3) Å. Similar Cu–S and Cu···Cu distances are observed for the polycrystalline hexanuclear compound **2** (R = *i*Bu, see Table 1). The mean Cu···Cu distance is much shorter than that reported in the crystallographic study by Liu et al.[8] The distances obtained with EXAFS are in agreement with the values from the structures of the polynuclear copper(I) *O*,*O*′-dialkyldithiophosphate clusters (discussed above) and it is unlikely that a mechanism would be present that could keep the copper ions separated by a distance of 3.129 Å in the $[Cu_6\{S_2P(OEt)_2\}_6]$ cluster compound, while allowing the overall ligand cage to shrink by 0.156 Å (compared with those for the $[Cu_8\{S_2P(OEt)_2\}_6(S)]$ cluster compound[9]).

Table 1. EXAFS mean distances *d*, Debye–Waller coefficients σ^2, and number of distances *N*, of the polynuclear copper(I) *O*,*O*′-dialkyldithiophosphate cluster compounds. The corresponding parameters obtained from crystallographic studies are given for comparison.[a]

Ligand tail R	Cluster L = R_2dtp	Average Cu···Cu distance XRD	EXAFS			Average Cu–S distance XRD	EXAFS			Average Cu···X_{center} distance (X = S^{2-}, Cl^-, Br^-) XRD	EXAFS		
			d [Å]	σ^2	*N*		*d* [Å]	σ^2	*N*		*d* [Å]	σ^2	*N*
*i*Pr[b]	Cu_4L_4	2.810	2.82(2)	0.023(2)	3	2.267	2.265(3)	0.0044(3)	3				
Et[c]	Cu_6L_6	3.129	2.85(3)	0.033(2)	3	2.250	2.266(3)	0.0061(3)	3				
*i*Bu (**2**)	Cu_6L_6	na	2.85(3)	0.032(2)	3	na	2.265(3)	0.0055(3)	3				
Et[d]	$Cu_8L_6(S)$[g]	3.009	3.01(3)	0.040(4)	3	2.305	2.293(3)	0.0065(4)	3	2.606	2.62(3)	0.032(4)	1
*n*Pr[e]	$Cu_8L_6(S)$[g]	3.011	3.02(3)	0.034(4)	3	2.302	2.294(3)	0.0090(4)	3	2.607	2.64(3)	0.032(4)	1
*i*Pr[c1]	$Cu_8L_6(S)$[g]	3.111	2.99(3)	0.044(3)	3	2.283	2.285(3)	0.0086(4)	3	2.694	2.64(2)	0.015(3)	1
*i*Bu (**1**)	$Cu_8L_6(S)$[g]	na	2.97(3)	0.047(4)	3	na	2.290(3)	0.0102(4)	3	na	2.63(2)	0.020(3)	1
*i*Pr[f]	$[Cu_8L_6Cl]PF_6$	3.112	na	na	na	2.283	na	na	na	2.695	na	na	na
*i*Pr[f]	$[Cu_8L_6Br]PF_6$	3.166	na	na	na	2.296	na	na	na	2.742	na	na	na

[a] na = not available. dtp = $S_2P(OiBu)_2$. [b], [c] and [c1], [d], [e], [f] The average XRD distances are obtained from the structures described in ref. [7,8,9,10,11], respectively. [g] The detailed simulations of EXAFS data for the $Cu_8L_6(S)$ compounds are shown in ref. [10].

The mean Cu···Cu distances in the hexameric *O*,*O*′-dialkyldithiophosphate cluster compounds, $[Cu_6\{S_2P(OR)_2\}_6]$ with R = alkyl, are expected to be longer than those in the $[Cu_4\{S_2P(OR)_2\}_4]$ cluster compounds due to the larger cluster, and shorter in comparison with the largest structure, the $[Cu_8\{S_2P(OR)_2\}_6(S)]$ type (see below).

The mean Cu–S bond lengths in $[Cu_4\{S_2P(O\textit{i}Pr)_2\}_4]$, $[Cu_6\{S_2P(OEt)_2\}_6]$, and **2** are very similar (Table 1), which is expected because of the identical chemical surroundings of the copper ions in these two structure types. The structural parameters for the $[Cu_6\{S_2P(OEt)_2\}_6]$ and **2** cluster compounds are almost identical, which strongly indicates that the structure of the $Cu_6(S_2P)_6$ core is independent of the length and branching of the alkyl chains.

The mean Cu–S bond lengths and the Cu···Cu distances in the $[Cu_8\{S_2P(OR)_2\}_6(S)]$ (R = Et, *n*Pr, *i*Pr, and *i*Bu) cluster compounds are slightly longer than those in the tetrameric and hexameric cluster compounds (Table 1) due to the fact that the copper(I) ions are tetracoordinated in the octameric clusters. The Cu–S bond lengths in the octanuclear $[Cu_8\{S_2P(OR)_2\}_6(S)]$ structures are slightly longer (by about 0.02 Å) relative to those in the tetranuclear, $[Cu_4\{S_2P(O\textit{i}Pr)_2\}_4]$, and hexanuclear, $[Cu_6\{S_2P(OR)_2\}_6]$ (R = Et and *i*Bu), cluster compounds. The bond to the central sulfide ion, $Cu–S_{center}$, is weaker in comparison with the bonds to the *O*,*O*′-dialkyldithiophosphate ions, which range from 2.6 to 2.7 Å in all reported octameric structures, $[Cu_8\{S_2P(OR)_2\}_6(S)]$.[8–12] The EXAFS data for the cluster compounds $[Cu_8\{S_2P(OR)_2\}_6(S)]$ (R = Et, *n*Pr, and *i*Pr) and **1** are almost identical, showing that the structure of the $Cu_8(S_2P)_6S$ core is also independent of the length and branching of the alkyl chains.[10] However, it must be stressed that even though the compounds are isostructural, the symmetry of the clusters decreases with increases in the length and branching of the alkyl chains, which is also seen in the space groups in which $[Cu_8\{S_2P(OR)_2\}_6(S)]$ cluster compounds crystallize (see above).

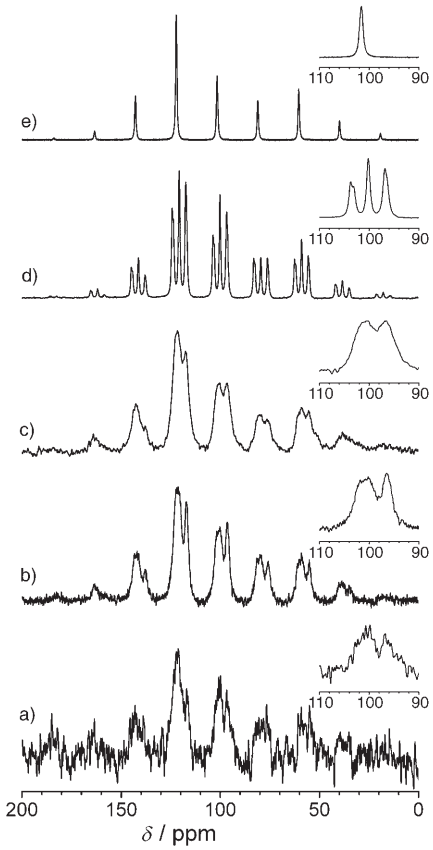

Figure 2. ^{31}P CP/MAS NMR spectra (at 8.46 T) of *O*,*O*′-diisobutyldithiophosphate compounds: surface-formed compounds on the synthetic chalcocite treated with a) 0.1, b) 1, and c) 10 mmol dm^{-3} aqueous solutions of $K[S_2P(O\textit{i}Bu)_2]$, 20000 signal transients; d) cluster compound **1** and e) cluster compound **2**, 32 signal transients. 3 kHz spinning frequency. Expanded regions with center bands are shown in the insets.

^{31}P CP/MAS NMR and SEM studies of 1 and 2: The ^{31}P CP/MAS NMR spectrum of the octanuclear cluster **1** is shown in Figure 2d. The compound displays three resonance lines (1:1:1) with isotropic shifts at δ_{iso} = 103.7, 100.2, and 96.8 ppm, and slight splitting of the two peripheral lines are observed (see the inset and Table 2). This means that the six *O*,*O*′-diisobutyldithiophosphate ligands are chemically almost equivalent in pairs.[16] It was found that the ^{31}P CP/MAS NMR spectrum of **1** (Figure 2d) was drastically changed by recrystallization in CH_2Cl_2 (Figure 2e). Instead of the three resonance lines, just one with an isotropic chemical shift at 101.6 ppm was observed, which suggests that the chemical environments for all of the phosphorus sites are very simi-

Table 2. ^{31}P chemical shift and chemical-shift anisotropy data (68.3% confidence limit) for the copper(I) *O*,*O*′-dialkyldithiophosphate cluster compounds.

Cluster compound	δ_{iso} [ppm]	δ_{aniso} [ppm]	η_{CS}	δ_{xx}	δ_{yy}	δ_{zz}	Ref.
1	103.7 (103.1) ± 0.1	−70.2 ± 1.2	0.50 ± 0.04	156.4 ± 1.7	121 ± 4	33.4 ± 1.0	[16]
	100.2 ± 0.1	−69.1 ± 1.2	0.2 ± 0.1	141.3 ± 3.5	127 ± 4	31.1 ± 1.0	
	96.8 (96.4) ± 0.1	−64.5 ± 0.8	0.1 ± 0.1	129.1 ± 1.6	129 ± 3	32.3 ± 1.0	
2	101.6 ± 0.1	−74.6 ± 0.5	0.34 ± 0.02	151.6 ± 1.8	126 ± 4	27.0 ± 1.0	this work
Surface-formed compounds[a]							
A	101.6 ± 0.5	−76.1 ± 1.7	0.38 ± 0.06	154 ± 5	125 ± 9	25 ± 5	this work
A	96.8 ± 0.5	−64.5 ± 1.0	0.1 ± 0.1	131 ± 4	127 ± 8	32 ± 5	
B	103.7 ± 0.5	−81 ± 7	0.3 ± 0.3	155 ± 12	133 ± 25	23 ± 5	
B	101.6 ± 0.5	−72 ± 5	0.2 ± 0.2	144 ± 7	131 ± 15	29 ± 5	
B	100.2 ± 0.5	−83 ± 13	0.4 ± 0.4	158 ± 19	125 ± 37	17 ± 13	
B	96.8 ± 0.5	−65 ± 4	0.3 ± 0.3	138 ± 9	120 ± 20	32 ± 4	
$K[S_2P(O\textit{i}Bu)_2]$	110.9 ± 0.2	−123.0 ± 2.0	0.0 ± 0.1	173 ± 9	172 ± 19	−12 ± 2	[25]

[a] Estimation of δ_{aniso} and η_{CS} for ^{31}P chemical sites was performed in two different ways: two (A) and four (B) sets of lines were used in the deconvolution procedures.

lar in this new copper(I) *O*,*O*′-diisobutyldithiophosphate cluster.

In our previous study we reported that the $[Cu_6\{S_2P(OEt)_2\}_6]$ cluster compound also displays a single resonance line in the ^{31}P CP/MAS NMR spectrum, with an isotropic shift at $\delta_{iso} = 101.0$ ppm and the ^{31}P chemical-shift anisotropy (CSA) parameters $\delta_{aniso} = -74.6$ ppm and $\eta_{CS} = 0.34$ (for comparison to the data in Table 2).[17] Based on the EXAFS data of **2** (see Table 1) and the similarity in the ^{31}P CSA data for $[Cu_6\{S_2P(OEt)_2\}_6]$ and **2**, the single ^{31}P resonance in the spectrum of **2** was assigned to the $[Cu_6\{S_2P(O\textit{i}Bu)_2\}_6]$ cluster compound.

Estimation of the ^{31}P CSA parameters, δ_{aniso} and η_{CS}, for **1** and **2** was based on the analysis of the spinning-sideband patterns in the NMR spectra obtained at three different spinning frequencies.[20] The results of the deconvolution and the subsequent evaluation of the CSA data are given in Table 2. The phosphorus sites in **2** ($\delta_{iso} = 101.6$ ppm) have more asymmetric ^{31}P chemical-shift tensors ($\eta_{CS} = 0.34$) than two of the P sites in **1** ($\delta_{iso} = 96.8$ and 100.2 ppm, $\eta_{CS} = 0.1$ and 0.2, respectively (Table 2)). The least deshielded resonance for **1** ($\delta_{iso} = 96.8$ ppm) has an almost axially symmetric tensor with η_{CS} close to zero.

The SEM images of compounds **1** and **2** are shown in Figure 3. After recrystallization in CH_2Cl_2, the needlelike structures of **1** (see Figure 3a) are not detected using a SEM microscope and only stacked polycrystalline polyhedra were observed (Figure 3b).

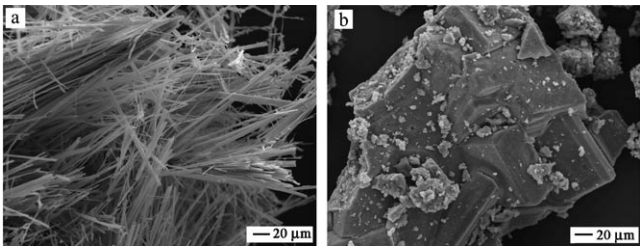

Figure 3. SEM images of cluster compounds a) **1** and b) **2** (**1** recrystallized in CH_2Cl_2).

Chemical effects of the recrystallization of 1: The recrystallization of **1** was performed by using CH_2Cl_2 (as previously mentioned), $CHCl_3$, CH_3I, and CCl_4 as solvents. The ^{31}P CP/MAS NMR spectra obtained for the samples after recrystallization in CH_3I and CCl_4 are shown in Figure 4a and b, respectively. The samples are mixtures of compounds **1** and **2**; the three resonance lines at $\delta_{iso} = 96.8$, 100.2, and 103.7 ppm (from **1**) are overlapped with the singlet (from **2**) at 101.6 ppm (see also Table 2). The corresponding SEM images of these samples are shown in Figure 5a and b. Compound **1** was recrystallized separately in EtOH/acetone (3:2 by volume) and toluene/cyclohexane (2:1) solvent mixtures and no compositional or structural changes were detected. However, only the resonance lines from **1** were observed in the ^{31}P CP/MAS NMR spectrum (not shown) after recrystal-

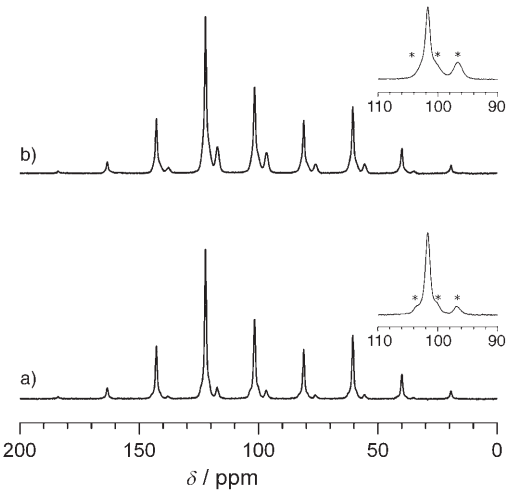

Figure 4. ^{31}P CP/MAS NMR spectra (at 8.46 T) of **1** recrystallized in a) CH_3I and b) CCl_4; 32 signal transients. 3 kHz spinning frequency. Expanded regions with center bands are shown in the insets. Traces of **1** are shown with asterisks.

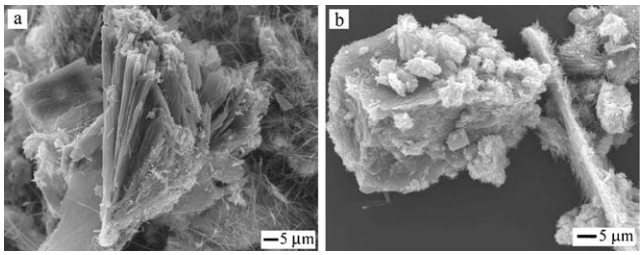

Figure 5. SEM images of **1** recrystallized in a) CH_3I and b) CCl_4.

lization in $CHCl_3$. This is probably due to the fact that the commercial product contains EtOH as a stabilizer. Attempts to separate the two phases (needlelike from polyhedral crystals) were unsuccessful.

Fackler and co-workers have suggested that the tetranuclear compound, $[Cu_4\{S_2P(OR)_2\}_4]$, undergoes an oxidation-induced transformation that results in cubanes with anions (such as S^{2-}, Cl^-, or Br^-) encapsulated in the cavity of the Cu_8 cage.[21] However, it is not clear how $[Cu_4\{S_2P(OR)_2\}_4]$ transforms into the final product, $[Cu_8\{S_2P(OR)_2\}_6(S)]$. The transformation from $[Cu_8L_6]^{4-}$ to $[Cu_6(S,L)_6]^{6-}$ with L = *i*MNT (isomaleonitrilethiolate, 1,1-dicyanoethylene-2,2-dithiolato) when powdered sulfur is added has been reported.[22]

The chemical reaction mechanisms with respect to the formation and recrystallization of compound **1** are not fully understood and have not yet been described. Evidently, the formation of compound **2** during the "recrystallization" of **1** does not include formation of Cu_2S, as it is very insoluble in the solvents used. It is most probable that additional *O*,*O*′-diisobutyldithiophosphate ions are required at the formation of **2** to achieve such a transformation. It is also evident that the S^{2-} (the center ion, involved in the formation of **1**) is a decomposition product of the *O*,*O*′-diisobutyldithiophos-

phate ion, which is the only source of sulfur in the synthesis, and it is known that in the formation of analogous molybdenum clusters the S^{2-} originates from the oxidized ligand ($R_2P(S)SS(S)PR_2$; R = alkyl).[19b] The hexameric copper(I) *O*,*O*′-diisobutyldithiophosphate (**2**) can only be formed by a partial decomposition of the octameric cluster compound **1**. The properties of the solvent used in the recrystallization/reformation reaction are certainly very important for the transformation reaction mechanisms, and thereby the most preferable cluster structure in a given solvent would be stabilized.

Powder X-ray diffraction study of 1 and 2: All our attempts to prepare single crystals of the aforementioned cluster compounds that would be suitable for X-ray diffraction measurements were unsuccessful. The obtained "needles" of **1** were extremely fragile (Figure 3a) and twinned. Samples of **1** and **2** were therefore additionally characterized using powder XRD analysis (see Figure 6a and 6b), which resulted

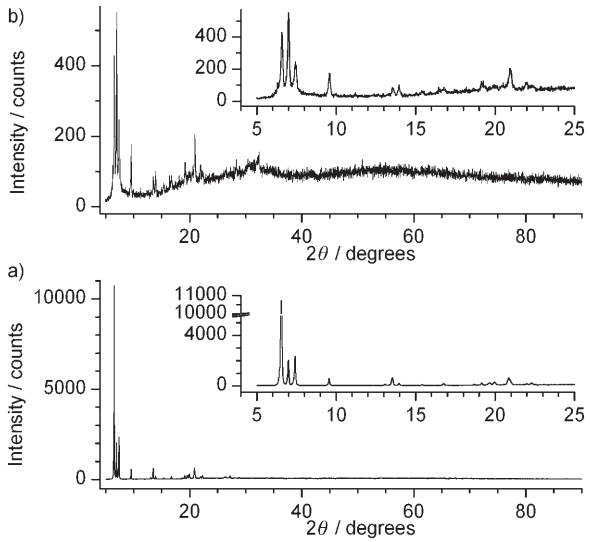

Figure 6. XRD powder patterns for a) **1** and b) **2**. Expanded regions (2θ = 5–25°) are shown in the insets.

in rather similar diffraction patterns, with the main differences occurring in the relative intensities of the first three reflections. Unexpectedly, the pattern obtained from **2** (i.e., **1** recrystallized in CH_2Cl_2) has a more amorphous character with a broad background (see Figure 6b), which is probably due to the presence of a large number of very small particles.[23]

Previous studies of $[Cu_8L_6(S)]$ and $[Cu_6L_6]$ (L = *O*,*O*′-diethyldithiophosphate) have shown that these two copper(I) cluster compounds contain almost-regular icosahedra of sulfur atoms. When all metal sites are fully occupied, the structure of the Cu_6S_{12} core in the $[Cu_6L_6]$ cluster corresponds to the cubane Cu_8S_{12} in $[Cu_8L_6(S)]$, without the center sulfur atom. Moreover, the S_{12}-icosahedral cage (L_6 cage) exhibits the same type of disorder also in the $[Zn_4L_6(S)]$ cluster in which four Zn atoms form a tetrahedron.[24] Calculations using the reported single-crystal structures[8–9] show that $[Cu_8L_6(S)]$ and $[Cu_6L_6]$ (L = *O*,*O*′-diethyldithiophosphate) have very similar diffractograms. Therefore, copper(I) cluster compounds with six *O*,*O*′-diisobutyldithiophosphate ligands but with different numbers of copper atoms in the core (six or eight), are expected to have similar XRD powder patterns (as seen in Figure 6a and b for the polycrystalline compounds **1** and **2**, respectively). It is reasonable to assume that they are crystallizing in the same or similar space groups, as has been seen for the ethyl analogues (see above).

^{65}Cu NMR spectroscopic study of 1 and 2: Solid-state static ^{65}Cu NMR experimental spectra for the central-transition region of **1** and **2** at 14.1 T are shown in Figures 7 and 8,

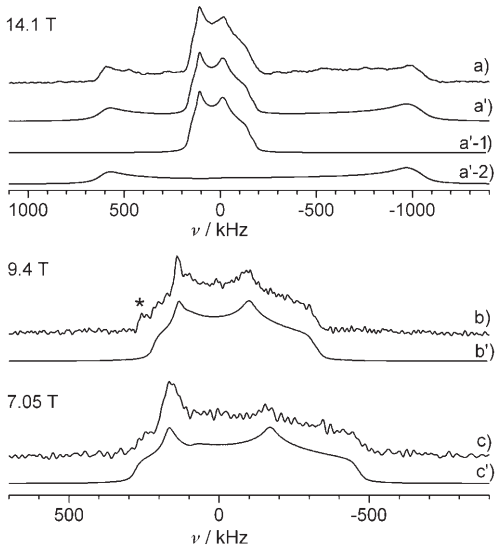

Figure 7. Solid-state static ^{65}Cu NMR spectra (at 14.1, 9.4, and 7.05 T) of cluster compound **1** (a–c), together with simulations (a′–c′); a′-1 and a′-2 show the individual line shapes used in a′. The broad component was not visible at 9.4 and 7.05 T. The probe background (at 9.4 T) is denoted with an asterisk.

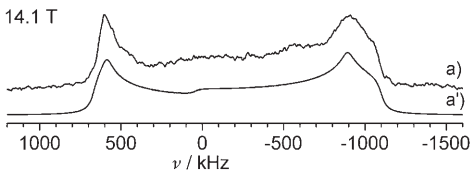

Figure 8. Solid-state static ^{65}Cu NMR spectrum (at 14.1 T) of cluster compound **2** (a), together with simulations (a′).

respectively, together with their corresponding simulations. ^{65}Cu NMR data for **1** at 9.4 and 7.05 T are also shown in Figure 7. Table 3 summarizes the NMR parameters used to simulate the ^{65}Cu static NMR spectra of these compounds.

Table 3. ^{65}Cu NMR parameters for copper(I) *O*,*O*′-diisobutyldithiophosphate cluster compounds **1** and **2**.[a]

	δ_{iso} [ppm]	C_Q [MHz]	η_Q ±0.02	δ_{aniso} [ppm]	η_{CS} ±0.02	ϕ [°]	χ (±1°)	ψ (±5°)	Integral intensity
1	410±20	19.3±0.1	0.40	450±30	0.00	–	10	65	0.48
	120±50	46.0±0.2	0.05	nd	nd	–	–	–	0.52
2	250±50	46.1±0.2	0.10	nd	nd	–	–	–	1

[a] nd = not detected; – = does not affect the line shape.

These parameters describe the two interaction tensors: the quadrupolar interaction (C_Q and η_Q) and the ^{65}Cu chemical-shift anisotropy (δ_{aniso} and η_{CS}).

In principle, a nuclear quadrupolar interaction takes place between a nucleus' quadrupole moment and the electric-field gradient (EFG), at its position, caused by the charge distribution around it. The size of the quadrupolar interaction experienced by a nucleus is described by the constant C_Q, whose value depends on the size of the EFG. The dependency of the EFG on nearby charges (typically up to several Ångströms) means that this quadrupolar interaction is sensitive to the number, position, and electronic configuration of the atoms surrounding the target nucleus. C_Q tends to have a smaller value when a nucleus is positioned at a site with a higher symmetry; in a cubic symmetry it is equal to zero. The asymmetry parameter, η_Q, shows the deviation of the EFG from the axial symmetry.

In our previous work on the hexanuclear $[Cu_6L_6]$ (L = $S_2P(OEt)_2$) cluster compound, only a single ^{65}Cu NMR resonance central-transition line shape with C_Q = 45.6 MHz was observed.[17] A similar broad (more than 10000 ppm or about 2000 kHz) second-order-type quadrupolar powder-pattern line shape with C_Q = 46.1 MHz was also observed in the solid-state static ^{65}Cu NMR spectrum of **2** (Figure 8). This means that in both the hexanuclear cluster compounds there is an overlap of six almost identical resonances (from six different copper sites), which indicates that the copper centers are situated at positions that experience almost identical local charge symmetry (having similar EFGs) and hence have similar quadrupolar constants, C_Q values.

The ^{65}Cu NMR spectrum of **1**, however, reveals two quadrupolar line shapes with relative intensities close to 1:1 (see Figure 7a and Table 3) suggesting the existence of two types of site with equal-sized populations.[16] These are substantially overlapped as the differences in isotropic chemical shift are much smaller than the quadrupolar line widths, as expected. The relative orientation dependence of the two interaction tensors (the chemical shift and quadrupolar interactions) for the narrower component of **1** (at 14.1 T) is reflected in the angle parameters (see Table 3). The accuracy of the parameters used to describe NMR data is increased by comparing powder spectra of **1** obtained at multiple magnetic-field strengths. This study provides more accurate values for the NMR interaction tensors and their relative orientations than that reported earlier.[16]

The presence of two quadrupolar line shapes with very different characteristics (see Table 3) is an indication of the presence of two copper centers with very different EFGs, despite the similarity in the local configuration. This indicates that the copper centers in the cube are coordinated in such a way that the local electronic charge distribution for one half of the sites is significantly different from the other half. Local electronic environments with higher symmetries tend to produce smaller EFGs and therefore quadrupolar line shapes that can be characterized by smaller values of C_Q. The line shape for compound **1** that is characterized by a smaller C_Q is therefore associated with such an electronic environment. For the copper sites in **1** displaying a weaker quadrupolar interaction (C_Q = 19.3 MHz, δ_{iso} = 410 ppm), ^{65}Cu CSAs are likely to be more comparable in strength with the second-order quadrupolar broadening, and a single static quadrupolar line shape was found to not adequately model the spectrum. The CSA interaction was consequently included in the simulations (see Table 3 and the Supporting Information). The sites with larger quadrupolar constants (C_Q = 46.0 MHz, δ_{iso} = 120 ppm) can be considered as a superposition of the copper sites in the core exhibiting electronic environments with lower symmetries.[16]

As mentioned earlier, the structure of the Cu_8S_{12}(S) fragment is independent of the type of alkyl chain but the symmetry of the cluster compounds decreases with increasing length and branching of the alkyl chains. The larger the ligand, the lower is the symmetry group in which the cluster compounds crystallize. Therefore, the local electronic configurations for the copper centers may change if a larger ligand is used (with R = *i*Bu in comparison with the R = *i*Pr), resulting in different EFGs being experienced by the copper centers.

The static solid-state ^{65}Cu NMR spectrum of **1** can therefore be considered as an example in which the eight copper sites with chemical environments of the same CuS_3···S type (as seen in the EXAFS data of **1**) display two different local electronic configurations. Due to the lack of structural data for **1**, the ^{65}Cu NMR spectrum was originally interpreted as a superposition of two quadrupolar line shapes, characterizing copper sites with different chemical environments (CuS_3 and CuS_3···S_{center}, respectively) originating from distortions of the Cu_8 cube.[16] The EXAFS data show unambiguously that the Cu_8 cube is 'equally distorted' in all octanuclear cluster compounds, $[Cu_8\{S_2P(OR)_2\}_6(S)]$ with R = Et, *n*Pr, *i*Pr, and *i*Bu, and all copper atoms are tetracoordinated (CuS_3···S).

It is notable, however, that the copper sites with larger quadrupolar constants (C_Q = 46.0 MHz) in **1** have similar EFGs to those in **2**, in which only the CuS_3-type chemical environment is present (the chemical environment with a lower symmetry relative to the pyramidal CuS_3···S type). This shows that very small differences in the local geometry of the copper sites in **1** are producing large differences in

the quadrupolar parameters, with corresponding differences in the electronic charge distribution.

The quadrupolar parameters (Table 3) provide relatively good fits to the spectra at 7.05, 9.4, and 14.1 T for the narrower line shape, and a fit for all three fields cannot be achieved without including the CSA component. However, the values for the broad line shapes in **1** and **2** are somewhat uncertain and would benefit greatly from higher field measurements (e.g., 21.1 T), where the strength of the ^{65}Cu CSA interaction is expected to be more similar to that of the second-order quadrupolar-interaction terms. The similarity is still somewhat surprising because EFGs are determined by local charge distributions and are therefore sensitive to the bonding characteristics for a site of interest, so the large differences in C_Q described above are indicative of significant differences in the bonding or bond strengths at the two sites, despite the apparent structural similarities found using other techniques in this study.

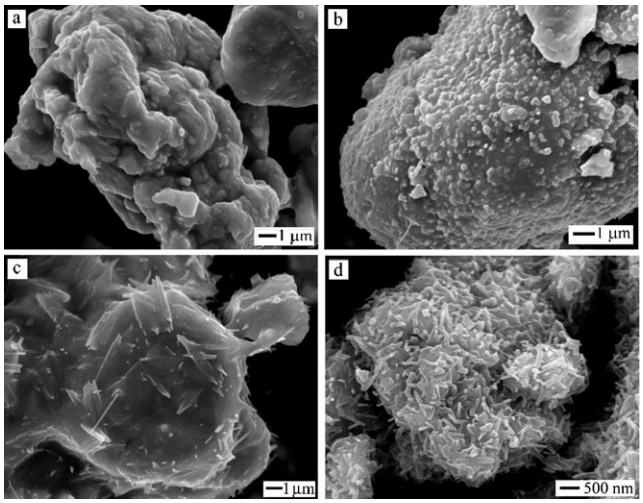

Figure 9. SEM images of a) a pure chalcocite, and chalcocite samples treated with b) 1, c) 5, and d) 10 mmol dm^{-3} K[$S_2P(OiBu)_2$].

Characterization of chalcocite surfaces after treatment with K[$S_2P(OiBu)_2$]—SEM and ^{31}P CP/MAS NMR studies: The ^{31}P CP/MAS NMR spectrum of synthetic chalcocite (Cu_2S) treated with a 0.1 mmol dm^{-3} aqueous solution of potassium *O*,*O*′-diisobutyldithiophosphate, K[$S_2P(OiBu)_2$], the lowest concentration of the collector used in this study, is shown in Figure 2a. Despite the high sensitivity for the ^{31}P nuclei ($I = {}^1/_2$, 100% natural abundance), the signal-to-noise ratio in the NMR spectrum of the sample was about 3:1 after accumulating 20000 signal transients. However, two broad resonance peaks (with isotropic shifts at about 101 and 96 ppm, and line widths of 5 and 3 ppm, respectively) flanked by spinning sidebands can be readily recognized. To assign these resonance lines, samples of chalcocite treated with higher concentrations of the collector (1 and 10 mmol dm^{-3}) were prepared (see Figure 2b,c). Higher concentrations of the ligand compound, K[$S_2P(OiBu)_2$], resulted in spectra with resonance lines at the same chemical shifts and with the same relative intensities (including the spinning sidebands) as for the 0.1 mmol dm^{-3} sample, but with improved signal-to-noise ratios. These observations indicate that the same *O*,*O*′-diisobutyldithiophosphate species are formed on the chalcocite surfaces at low and high concentrations of the collector, with increasing amounts of these species at higher collector concentrations.

The SEM images of the surfaces of synthetic chalcocite used in this study, before and after the treatment with K[$S_2P(OiBu)_2$] at different concentrations (1, 5, and 10 mmol dm^{-3}), are shown in Figure 9. The initially smooth chalcocite surface was only slightly affected when using a low concentration of *O*,*O*′-diisobutyldithiophosphate during the conditioning of the sample (Figure 9b). At medium-low concentrations (5 mmol dm^{-3} K[$S_2P(OiBu)_2$], Figure 9c), needlelike structures were observed on the surface. When the concentration of the ligand was doubled (10 mmol dm^{-3}) the needlelike structures became more abundant, covering the entire surface (Figure 9d). The sample treated with the most dilute solution of K[$S_2P(OiBu)_2$] (0.1 mmol dm^{-3}, not shown), did not show any changes in morphology, although the ^{31}P CP/MAS NMR spectrum revealed the presence of the same *O*,*O*′-diisobutyldithiophosphate species (as discussed above). Both SEM and ^{31}P NMR spectroscopic data indicate that the type of polycrystalline *O*,*O*′-diisobutyldithiophosphate species formed at the surface of synthetic chalcocite is independent of the collector concentration in the range 0.1–10 mmol dm^{-3}.

It was noticed that the isotropic ^{31}P chemical shifts of the phosphorus sites in the cluster compound **1** are very similar to those detected for the collector-treated chalcocite surfaces (see Table 2). Furthermore, similarities in the spinning-sideband patterns (compare Figure 2b,d) indicate that the chemical-shift anisotropies of the P sites in compound **1** are similar to those for the species formed on the mineral surface. To more accurately assign the two broad ^{31}P resonance lines in the NMR spectra of the substances formed on the chalcocite surfaces (see Figure 2b,c) these spectra were deconvoluted in two different ways (using either two or four sets of resonance lines) using the spectrometer's in-built Spinsight program. A comparative data analysis (of both ^{31}P isotropic chemical shifts and ^{31}P CSAs) confirms the existence of two dominating copper(I) *O*,*O*′-diisobutyldithiophosphate polynuclear species (**1** and **2**) at the Cu_2S surfaces. Furthermore, the ratio of the relative amounts of **1** and **2** on the mineral surfaces was estimated to be 0.7:0.3 (as calculated from the intensities of the spinning sidebands when the spectrum was deconvoluted using a set of four lines, see row (B) in Table 2). The ^{31}P CSA parameter δ_{aniso} varies between −64 and −80 ppm for both the individual cluster compounds and the species formed on the mineral surface, thus confirming the presence of just bridging-type coordination of the ligands in these copper(I) *O*,*O*′-diisobutyldithiophosphate species.[25] The large uncertainty in these data is due to the noise level in the spectra, an overlap of the broad resonance lines, and the poorer resolution for the higher-order spinning sidebands.

The solubility product of chalcocite is very low (pK_{SP} = 53).[26] In spite of this fact, a very small amount of copper(I) ions will be dissolved and quickly oxidized to copper(II) in the presence of water. This process allows additional copper(I) ions to be released and oxidized until an equilibrium is reached. However, in the presence of *O*,*O*′-dialkyldithiophosphate, the copper(II) ions will be reduced to copper(I) during the formation of copper(I) *O*,*O*′-dialkyldithiophosphate cluster compounds accompanied by the oxidation of *O*,*O*′-dialkyldithiophosphate ions to bis(dialkylthiophosphoryl) disulfide.[27] Recent studies have shown that copper atoms at a chalcocite surface can react with the formed disulfide molecules to form more copper(I) *O*,*O*′-dialkyldithiophosphate species.[28] The fact that no traces of disulfides were observed in the ^{31}P NMR spectra of any of the collector-treated Cu_2S samples is therefore a further indication of the existence of this process. As these reactions take place in very close vicinity to the chalcocite surface, the aforementioned compounds will be formed as an extension of the surface as can be seen in the SEM images. A similar interaction mechanism could be considered for ZnS surfaces when sphalerite is activated by copper(II) ions prior to the flotation process.

It is worth noting that adsorption of *O*,*O*′-dialkyldithiophosphate ligands could also occur prior or parallel to the oxidation process (Cu^{I} to Cu^{II}). This has been observed in ^{31}P CP/MAS spectra when nonactivated synthetic sphalerite and *O*,*O*′-dialkyldithiophosphate ligands were applied.[18] However, such a primary reaction product was not detected in the ^{31}P CP/MAS NMR spectra of the collector-treated chalcocite surfaces studied here.

Conclusion

The structural relationships between the polycrystalline cluster compounds Cu_4L_4, Cu_6L_6, and $Cu_8L_6(S)$ (L = $S_2P(OR)_2$ with R = alkyl) were studied by copper K-edge EXAFS. It was shown that by increasing the nuclearity of the clusters a proportional increase in the Cu···Cu distance occurs. The Cu–S bond length is the same in the Cu_4L_4 and Cu_6L_6 clusters because of the identical chemical environments of the copper ions (CuS_3), but slightly longer (by ca. 0.02 Å) in the $Cu_8L_6(S)$ clusters due to the tetracoordinated copper(I) ions (CuS_3···S). It was also found that the structures of the $Cu_6(S_2P)_6$ and $Cu_8(S_2P)_6(S)$ cores are independent of the length and branching of the alkyl chains. The polycrystalline copper(I) *O*,*O*′-diisobutyldithiophosphate cluster compounds, $[Cu_8\{S_2P(OiBu)_2\}_6(S)]$ and $[Cu_6\{S_2P(OiBu)_2\}_6]$, were characterized using ^{31}P CP/MAS and static ^{65}Cu (at multiple magnetic-field strengths) solid-state NMR spectroscopies, powder XRD, SEM, and EXAFS analyses. The ^{31}P and ^{65}Cu isotropic and anisotropic chemical shifts and ^{65}Cu quadrupolar interaction parameters for $[Cu_8\{S_2P(OiBu)_2\}_6(S)]$ and $[Cu_6\{S_2P(OiBu)_2\}_6]$ cluster compounds were estimated by simulating the experimental NMR spectra. The adsorption mechanism of potassium *O*,*O*′-diisobutyldithiophosphate on the surface of synthetic chalcocite was studied by means of solid-state ^{31}P CP/MAS NMR spectroscopy and SEM analysis. From these data, it was concluded that the same species were formed at synthetic chalcocite surfaces in the collector concentration range used (0.1–10 mmol dm^{-3}). The ^{31}P chemical-shift data (both isotropic chemical shifts and CSAs) for substances formed at the synthetic chalcocite surfaces allowed the assignment of these species to a mixture of $[Cu_8L_6(S)]$ and $[Cu_6L_6]$ (L = $S_2P(OiBu)_2$) compounds. These are formed in a reaction where copper(I) from the chalcocite is oxidized to copper(II), before being reduced back to copper(I) in copper(I) *O*,*O*′-diisobutyldithiophosphate cluster compounds.

Experimental Section

Materials: Copper(I) chloride (CuCl) and all solvents (analytical grade) were obtained from Merck. *N*,*N*′-Dimethylformamide (DMF) and dichloromethane (CH_2Cl_2) were distilled before use. Potassium *O*,*O*′-dialkyldithiophosphate ligands, $K[S_2P(OEt)_2]$, $K[S_2P(OnPr)_2]$, $K[S_2P(OiPr)_2]$, and $K[S_2P(OiBu)_2]$, the commercial collectors Danafloat 123K, 133K, 233K, and 245K, respectively, were provided by CHEMINOVA AGRO A/S and used as received. Synthetic chalcocite, Cu_2S, was obtained from STREM CHEMICALS. The structural identity of the chalcocite was confirmed using X-ray powder diffraction data.

Synthesis and characterization of the cluster compounds

$[Cu_4\{S_2P(OiPr)_2\}_4]$ and $[Cu_6\{S_2P(OEt)_2\}_6]$: The polycrystalline cluster compounds were obtained by following the methods of Kokotailo et al.[7]and Liu et al.,[8] respectively, and were characterized as reported elsewhere.[16]

$[Cu_8\{S_2P(OR)_2\}_6(S)]$ (R = Et, n*Pr,* i*Pr)*: The polycrystalline cluster compounds were obtained using the method of Matsumato et al.[9] and characterized as reported earlier.[10]

*$[Cu_8\{S_2P(OiBu)_2\}_6(S)]$ (**1**)*: The cluster compound was prepared by reacting CuCl (1 mmol) and $K[S_2P(OiBu)_2]$ (1 mmol) in DMF, also following the method of Matsumato et al.[9] The mixture was left for 24 h at RT under stirring, allowing the CuCl to dissolve. The solution was filtered and left for a spontaneous crystallization to take place in an open vessel at RT for 3–4 d. Fine white needlelike crystals were obtained (40 % yield). These were collected, dried, and recrystallized separately in an EtOH/acetone mixture (3:2), a toluene/cyclohexane mixture (2:1), and finally in halogen-containing solvents (CCl_4, CH_3Cl, CH_2Cl_2, CH_3I). M.p. 204–205 °C. The FAB mass spectrum for a freshly prepared sample showed a peak at m/z = 1990 for the S-centered cluster, $[Cu_8\{S_2P(OiC_4H_9)_2\}_6SH]^+$, and a strong peak at m/z = 977, consistent with the formation of $[Cu_4\{S_2P(OiC_4H_9)_2\}_3]$ fragments. S/P elemental ratio calcd for $C_{48}H_{108}Cu_8O_{12}P_6S_{13}$ (M_r = 1988.36): 2.24; found: 2.23.

*$[Cu_6\{S_2P(OiBu)_2\}_6]$ (**2**)*: The cluster compound was obtained by recrystallizing $[Cu_8\{S_2P(OiBu)_2\}_6(S)]$ (**1**) in freshly distilled CH_2Cl_2. This compound was also independently obtained as a main product using the synthesis procedure reported by Liu et al. (with $K[S_2P(OiBu)_2]$ being used instead of the $NH_4[S_2P(OiBu)_2]$ salt and with $[Cu(CH_3CN)_4]PF_6$ as a source of copper(I)).[8] In the latter synthesis, traces of **1** were also found in the ^{31}P CP/MAS spectrum, while no traces of PF_6^- anions were observed indicating that no PF_6^- anions were incorporated in the lattice of the obtained compound. S/P elemental ratio calcd for $C_{48}H_{108}Cu_6O_{12}P_6S_{12}$ (M_r = 1829.21): 2.07; found: 2.08.

The elemental analysis for **1** and **2** was performed at Mikrokemi AB, Uppsala, according to procedures described on their homepage: http://www.mikrokemi.se/.

Surface-formed compounds: 1 g of synthetic chalcocite (Cu_2S) powder was immersed in an aqueous solution (50 mL) of $K[S_2P(OiBu)_2]$ at pH 9.2 (borate buffer) and kept under stirring for 30 min. The ligand was

dissolved in deionized water, and after conditioning, the samples were centrifuged at 4000 rpm for 5 min, rinsed with deionized water, centrifuged once more, and dried in a vacuum desiccator. In this study, the aqueous solutions used were in the concentration range 0.1–10 mmol dm^{-3} $K[S_2P(OiBu)_2]$. The procedure was repeated using a dilute aqueous solution of KOH (instead of the borate buffer) to adjust the pH to 9.2 and no change in the ^{31}P CP/MAS NMR results was observed. The synthetic chalcocite has a specific surface area of about 1 m^2g^{-1}.

Analytical methods

General: All experiments were performed at ambient temperature (298 K).

^{31}P CP/MAS NMR spectroscopy: Solid-state ^{31}P MAS NMR spectra were recorded at 145.73 MHz on a Varian/Chemagnetics Infinity CMX-360 (B_0 = 8.46 T) spectrometer with cross polarization (CP) from the protons and proton decoupling.[29] The CP mixing time was 3 ms. The ^1H 90° pulse width was 5 μs. 32 (for the pure compounds) and 20000 signal transients (for the surface compounds) were accumulated with 3 s relaxation delays. The samples were packed in standard ZrO_2 rotors: 4 mm for the pure cluster compounds and 7.5 mm for the surface compounds. To increase the reliability of the simulations of the chemical-shift anisotropy parameters, the ^{31}P NMR spectra were obtained at three different spinning frequencies (3–5 kHz). The spectra were externally referenced to 85.5 % H_3PO_4.[30]

By analyzing the intensities of the spinning sidebands in the ^{31}P spectral patterns, the CSA parameters (δ_{aniso} and η_{CS}) for the copper(I) *O,O′*-dialkyldithiophosphate cluster compounds were estimated. A simulation program in the Mathematica front-end was used for this purpose. The calculations involved the integrated intensities of the spinning sidebands, the Larmor resonance frequency, the spinning frequency, and the noise-level variance.[20]

Static ^{65}Cu NMR spectroscopy: The ^{63}Cu and ^{65}Cu isotopes both have spin $I = {}^3/_2$ and large quadrupole moments. Despite the lower natural abundance of the ^{65}Cu isotope, it was preferred in this study, because its resonance frequency falls in a spectral window that is relatively free from other isotopes and the effect of the quadrupolar interaction is slightly smaller. Excitation at a single frequency was insufficient to excite the whole central-transition spectrum because of the width of the powder line shapes, and the spectra were therefore acquired by repeatedly stepping the carrier frequency by 100 kHz, retuning the probe and acquiring a new set of data, before finally adding all the sub-spectra together.[31]

The solid-state ^{65}Cu NMR spectra of **1** and **2** were recorded at 170.40 MHz on a Varian/Chemagnetics Infinity CMX-600 spectrometer equipped with a wide-bore 14.1 T magnet. The static spectra were collected using a Bruker 5 mm static probe. In all cases, a spin-echo pulse sequence was utilized (1.1 μs–τ–1.1 μs, τ = 15 μs). The spectra were obtained with a pulse delay of 40 ms and 50000 transients were averaged. The solid-state ^{65}Cu NMR spectra of **1** were also recorded at two additionally applied magnetic field strengths: at 7.05 T using a Bruker CXP-300 spectrometer, and at 9.4 T, using a Bruker MSL-400 spectrometer. The reference frequencies for ^{65}Cu were 85.20 and 113.62 MHz, respectively. The spectra were acquired using Bruker 7 mm static probes and spin-echo pulse-sequence experiments. At 9.4 T, the radio-frequency field strength, B_1, was 116 kHz, the pulse timings were (1.0 μs–τ–1.0 μs, τ = 20 μs) with 0.5 s relaxation delays, and 40960 transients were averaged per resonance offset. At 7.05 T, B_1 was 125 kHz, the same experimental timings as those for 9.4 T were used, and 170000 transients were averaged per resonance offset. The ^{65}Cu NMR spectra at 7.05 and 9.4 T were obtained in a similar way to those for 14.1 T, with the transmitter frequency being stepped by increments of 100 kHz. The energy-level splittings that are utilized in NMR spectroscopy are smaller at lower field strengths, and the resulting weaker signal strengths are exacerbated further by the broader width of spectra such as those studied here. The range of transmitter frequencies used was therefore limited to those in the region of line shapes with smaller quadrupolar coupling constants and therefore narrower widths. All ^{65}Cu NMR spectra were externally referenced to a secondary standard of powdered CuCl at δ = 0 ppm.[32]

These NMR data were processed with the free induction decay (FID) data left-shifted to the echo maximum prior to the Fourier transform (FT) (half echo). The second-order quadrupolar line shapes for the central transition of ^{65}Cu nuclei, including a chemical-shift anisotropy (CSA) contribution where necessary, were simulated by using the DMfit program.[33] The errors were estimated by changing the value of one parameter when all of the other parameter values were kept constant. Furthermore, the ^{65}Cu NMR spectra were simulated using the SIMPSON simulation program[34] to confirm independently the NMR parameters obtained by DMFit.

EXAFS measurements: 20 mg of each solid compound $[Cu_4\{S_2P(OiPr)_2\}_4]$, $[Cu_6\{S_2P(OEt)_2\}_6]$, $[Cu_8\{S_2P(OR)_2\}_6(S)]$ (R = Et, *n*Pr, and *i*Pr), **1**, and **2** were diluted in 25 mg boron nitride (BN), and carefully grained, to give an edge step in the transition mode of approximately one unit in the logarithmic intensity ratio. The cell was a 1 mm aluminum frame with Mylar tape windows.

Copper K-edge EXAFS measurements were performed at the wiggler beam line I811 at the MAXII Synchrotron, the MAX Laboratory, Lund University, Sweden. The EXAFS station was equipped with a Si(111) double-crystal monochromator and higher-order harmonics were reduced by detuning the second monochromator crystal to reflect 60 % of the maximum intensity at the end of the scans. The internal-energy calibration was made with a copper metal foil with the first inflection point assigned to 8980.3 eV.[35] The experiments were performed in transmission mode at ambient temperature. Two scans (with a recording time of 90 min for each scan) were averaged to give a good data quality in the k range 2–16 $Å^{-1}$ (k^3-weighted data), for which $k = \sqrt{0.2625(E-E_0)}$, where E is the actual energy and E_0 is the threshold energy of the adsorption edge. Calculated model functions using ab initio calculated phase and amplitude parameters obtained by the FEFF7 and GNXAS programs were curve-fitted in k space.[36]

The EXAFSPAK and GNXAS program packages were used for the data treatment. The data analyses were performed by means of the GNXAS code in order to obtain the best possible splines. The GNXAS code is based on the calculation of the EXAFS signal and a subsequent refinement of the structural parameters.[37] The GNXAS method accounts for multiple scattering (MS) paths, with correct treatment of the configurational average of all the MS signals to allow the fitting of correlated distances and bond-length variances (Debye–Waller factors). A correct description of the first coordination sphere of the studied compound has to account for asymmetry in the distribution of the absorber–scatterer distances.[38] Therefore the Cu–S two-body signals associated with the first coordination shells were modeled with Γ-like distribution functions that depend on four parameters, namely the coordination number N, the average distance R, the mean-square variation σ, and the skewness β. The β term is related to the third cumulant C_3 through the relation $C_3 = \sigma^3\beta$. However, the β term was negligible for all distances of importance in this study. R is the first moment of the function $[4\pi(g(r))^{-2}]dr$, in which g = splitting factor and r = distance.

The standard deviations given for the refined parameters in Table 1 are obtained from k^2-weighted least-squares refinements of the EXAFS function $\chi(k)$, and do not include systematic errors of the measurements. These statistical error estimates provide a measure of the precision of the results and allow various reasonable comparisons, including the significance of relative shifts in the distances. However, the variations in the refined parameters, including the shift in the E_0 value (for which k = 0), using different models and data ranges, indicate that the absolute accuracy of the distances given for the separate complexes is within ±0.01–0.02 Å for well-defined interactions. The "standard deviations" given in the text have been increased accordingly to include the estimated additional effects of systematic errors.

SEM images: The morphologies of the samples were studied with a Philips XL 30 scanning electron microscope equipped with a LaB_6 emission source. A Link ISIS Ge energy-dispersive X-ray detector (EDS) attached to the SEM was used to additionally probe the composition of the polycrystalline copper(I) *O,O′*-dialkyldithiophosphate cluster compounds.

Surface-area determination: A chalcocite sample was degassed at 575 K overnight and nitrogen-adsorption measurements were performed on a Micromeritics ASAP 2010 instrument. The specific surface area was calculated using the BET equation.[39]

X-ray powder diffraction: X-ray powder diffraction patterns were collected using a Siemens D5000 diffractometer and $Cu_{K\alpha}$ radiation, λ = 1.5418 Å.

Acknowledgements

The work was financed by the Agricola Research Centre at Luleå University of Technology and the Marie Curie Industry Host Fellowship (HPMT-CT-2001-00335-02). The Varian/Chemagnetics Infinity CMX-360 spectrometer was purchased with a grant from the Swedish Council for Planning and Coordination of Research (FRN) and further upgraded with a grant from The Foundation to the memory of J. C. and S. M. Kempe. The EXAFS data were carried out at MAXLab, University of Lund, and supported by The Swedish Research Council and The Wallenberg Foundation. The MAXLab, Lund University, is gratefully acknowledged for allocation of beam time and putting laboratory facilities at our disposal. MAXLab is supported by The Swedish Research Council and The Knut and Alice Wallenbergs Stiftelse, and additional support was given by The Crafoordska Stiftelse and The Faculty of Science & Technology, Norwegian University of Science & Technology. We are grateful to Marshall Hughes, of the Organic Mass Spectroscopy Facility in the CSL at the University of Tasmania, for the FAB mass measurements of the cluster compounds. The authors also acknowledge CHEMINOVA AGRO A/S for the dithiophosphate reagents. We thank Dr. Andy Howes, Professor Mark E. Smith, University of Warwick, UK, and Dr. Mats Lindberg, Luleå University of Technology, Sweden, for discussions, and we are grateful for the support from Dr. Stefan Carlson at the MAXLab.

[1] I. A. Kabovski, *Proc. Int. Congr. Surf. Act., 2nd*, **1957**, *2*, 222–228.
[2] G. Scott, *Atmospheric Oxidation and Antioxidants*, Elsevier, Amsterdam, **1965**.
[3] G. S. Hartley, T. F. West, *Chemicals for Pest Control*, Pergamon, New York, **1969**.
[4] J. Stary, *The Solvent Extraction of Metal Complexes*, Pergamon, New York, **1964**.
[5] N. D. Yordanov, V. Alexiev, J. Macicek, T. Glowiak, D. Russel, *Transition Met. Chem.* **1983**, *8*, 257–261.
[6] D. Wu, J. Q. Huang, Y. Lin, J. L. Huang, *Sci. Sin. Ser. B (Engl. Ed.)* **1988**, *31*, 800–806.
[7] S. L. Lawton, W. J. Rohrbaugh, G. T. Kokotailo, *Inorg. Chem.* **1972**, *11*, 612–618.
[8] C. W. Liu, T. Stubbs, J. P. Fackler, Jr., *J. Am. Chem. Soc.* **1995**, *117*, 9778–9779.
[9] K. Matsumato, R. Shimomira, Y. Nakao, *Inorg. Chim. Acta* **2000**, *304*, 293–296.
[10] D. Rusanova, K. E. Christensen, I. Persson, K. J. Pike, O. N. Antzutkin, X. Zou, R. Dupree, W. Forsling, submitted to *J. Cluster Sci.* **2006**.
[11] C. W. Liu, M. D. Irwin, A. A. Mohamed, J. P. Fackler, Jr., *Inorg. Chim. Acta* **2004**, *357*, 3950–3956.
[12] Y.-B. Chen, Z.-J. Li, Y.-Y. Qin, Y. Kang, J.-K. Cheng, R.-F. Hu, Y.-H. Wen, Y.-G Yao, *Inorg. Chem. Commun.* **2003**, *6*, 405–407.
[13] R. Woods, D. S. Kim, R. H. Yoon, *Int. J. Miner. Process.* **1993**, *39*, 101–106.
[14] J. S. Hanson, D. W. Fuerstenau, *Int. J. Miner. Process.* **1991**, *33*, 33–47.
[15] M. Valli, B. Malmsten, I. Persson, *Colloids Surf. A* **1994**, *83*, 227–236.
[16] D. Rusanova, W. Forsling, O. N. Antzutkin, K. J. Pike, R. Dupree, *J. Magn. Reson.* **2006**, *179*, 10–15.
[17] D. Rusanova, W. Forsling, O. N. Antzutkin, K. J. Pike, R. Dupree, *Langmuir* **2005**, *21*, 4420–4424.
[18] a) A. V. Ivanov, O. N. Antzutkin, A.-C. Larsson, M. Kritikos, W. Forsling, *Inorg. Chim. Acta* **2001**, *315*, 26–35; b) A.-C. Larsson, O. N. Antzutkin, A. V. Ivanov, W. Forsling, *Proceedings Centenary of Flotation Symposium*, The Australasian Institute of Mining and Metallurgy, Melbourne, **2005**, pp. 497–505.
[19] a) I. Haiduc, D. B. Snowerby, S.-F. Lu, *Polyhedron* **1995**, *14*, 3389–3472; b) I. Haiduc, L. Y. Goh, *Coord. Chem. Rev.* **2002**, *224*, 151–170.
[20] O. N. Antzutkin, Y. K. Lee, M. H. Levitt, *J. Magn. Reson.* **1998**, *135*, 144–155.
[21] J. P. Fackler, Jr., C. W. Liu, R. J. Staples, R. T. Stubbs, *Abstr. Pap. Am. Chems.* 216:334, Part 2, Aug 23, **1998**.
[22] C. W. Liu, R. J. Staples, J. P. Fackler, Jr., *Coord. Chem. Rev.* **1998**, *174*, 147–177.
[23] E. P. Bertin, *Introduction to X-ray Spectrometric Analysis*, Plenum Press, New York, **1978**.
[24] J. P. Fackler, Jr., R. J. Staples, C. W. Liu, R. T. Stubbs, C. Lopez, J. T. Pitts, *Pure Appl. Chem.* **1998**, *70*, 839–844.
[25] A.-C. Larsson, A. V. Ivanov, W. Forsling, O. N. Antzutkin, A. E. Abraham, A. C. de Dios, *J. Am. Chem. Soc.* **2005**, *127*, 2218–2230.
[26] I. Persson, *J. Coord. Chem.* **1994**, *32*, 261–242.
[27] N. D. Yordanov, *Transition Met. Chem.* **1997**, *22*, 200–207.
[28] A. N. Buckley, S. W. Goh, R. N. Lamb, R. Woods, *Int. J. Miner. Process.* **2003**, *72*, 163–174.
[29] A. Pines, M. G. Gibby, J. S. Waugh, *J. Chem. Phys.* **1972**, *56*, 1776–1777.
[30] R. K. Harris, *Encyclopedia of Nuclear Magnetic Resonance, Vol. 6*, Wiley, New York, **1996**, p. 3612.
[31] T. J. Bastow, M. E. Smith, *Solid State Nucl. Magn. Reson.* **1992**, *1*, 165–169.
[32] K. J. D. Mackenzie, M. E. Smith, K. J. E. Dunn, *Multinuclear Solid-State Nuclear Magnetic Resonance of Inorganic Materials*, Pergamon, Amsterdam, **2002**.
[33] D. Massiot, F. Fayon, M. Capron, I. King, S. Le Calvé, B. Alonso, J.-O. Durand, B. Bujoli, Z. Gan, G. Hoatson, *Magn. Reson. Chem.* **2002**, *40*, 70–76; DMfit program available at http://crmht-europe.cnrs-orleans.fr/.
[34] M. Bak, J. T. Rasmussen, N. C. Nielsen, *J. Magn. Reson.* **2000**, *147*, 296–330; http://nmr.imsb.au.dk/bionmr/software/simpson.php/.
[35] A. Thompson, D. Attwood, E. Gullikson, M. Howells, K.-J. Kim, J. Kirz, J. Kortright, I. Lindau, P. Pianatta, A. Robinson, J. Scofield, J. Underwood, D. Vaughan, G. Williams, H. Winick, *X-ray Data Booklet*, LBNL/PUB-490 Rev. 2, Lawrence Berkeley National Laboratory, Berkeley, California 94720, **2001**.
[36] a) S. I. Zabinsky, J. J. Rehr, A. Ankudinov, R. C. Albers, M. J. Eller, *Phys. Rev. B* **1995**, *52*, 2995–3009; b) A. L. Ankudinov, J. J. Rehr, *Phys. Rev. B* **1997**, *56*, R1712–R1715; the FEFF program is available at http://feff.phys.washington.edu/feff/.
[37] A. Filipponi, A. Di Cicco, *Phys. Rev. A* **1995**, *52*, 1072–1078.
[38] a) A. Filipponi, *J. Phys.: Condens. Matter*, **1994**, *6*, 8415–8427; b) L. Hedin, B. I. Lundqvist, *J. Phys. C* **1971**, *4*, 2064.
[39] S. J. Gregg, K. S. W. Sing, *Adsorption, Surface Area and Porosity*, Academic Press, London, **1982**.

Received: November 30, 2005
Published online: March 10, 2006

